VI International Conference on Computational Methods for Coupled Problems in Science and Engineering
COUPLED PROBLEMS 2015
B. Schrefler, E. Oñate and M. Papadrakakis(Eds)

COMPARISON OF ADVANCED TURBULENCE MODELING APPROACHES FOR FLUID-STRUCTURE INTERACTION

A. Ali*†, T. Reimann†, D.C. Sternel† and M. Schäfer†

†Institute of Numerical Methods in Mechanical Engineering
Technische Universität Darmstadt
Dolivostraße 15, 64293 Darmstadt, Germany
e-mail: ali@fnb.tu-darmstadt.de, web page: http://fnb.tu-darmstadt.de

Key words: Fluid-Structure Interaction, Turbulence, Delayed Detached-Eddy Simulation, Large Eddy Simulation

Abstract. In this study we present the results of the benchmark of a turbulent Fluid-Structure Interaction test case. An implicit partitioned approach is employed to couple the fluid and structure subproblems. We employ three different techniques to model the turbulence in fluid motion. A 2-d unsteady Reynolds Averaged Navier-Stokes approach, with an elliptic relaxation based turbulence model ($\zeta - f$), successfully captures the oscillation mode. Further investigations are performed with a Delayed Detached Eddy Simulation and a Large Eddy Simulation model. The $\zeta - f$ model is used as a baseline unsteady Reynolds Averaged Navier-Stokes model for the Delayed Detached Eddy Simulation. A comparison of the structural deflections from the simulations show a reasonable agreement with the experiment. In light of the presented results, the suitability of the modeling approaches is discussed.

1 INTRODUCTION

Fluid-Structure Interaction (FSI) phenomena are important to study the design of many engineering applications. Experiments for most of the real-world FSI applications are not feasible – measurement techniques can not look inside all the important parameters, and are too expensive. With increasing computational power, simulation of such multi physics scenarios are becoming feasible and can give new knowledge. The capabilities of these numerical methods to study FSI needs to be validated against benchmark test cases.

A great number of FSI applications have turbulent fluid motion, thus making it important to study the FSI phenomena in turbulent flows. The numerical and experimental studies on FSI, conducted in the last decade mostly focused on laminar flows. In an effort

to provide experimental data for validation of numerical tools, Gomes and Lienhart [6] proposed the first validation test case for FSI with incompressible turbulent fluid motion. The structural model of this test case, contains a thin flexible sheet attached to a revolvable cylinder with a rectangular mass attached to the other end of the sheet. The structure is placed inside a vertical tunnel with the flow *Reynolds Number* (R_e) of 15,000, based on the cylinder diameter. The structure exhibits a periodic oscillation close to its natural frequency. This instability mechanism is characterized as *Instability Induced Excitation* (IIE) [14] with the structure swiveling in the first mode.

Recently De Nayer and Kalmbach [4], as well as Kalmbach and Breuer [11] have proposed two different test cases with turbulent fluid motion. The proposed benchmark test cases offer a simpler structure geometry and provide a different excitation mechanism and motion mode, which is not present in [6]. The R_e based on the cylinder diameter is in sub-critical regime [15] ($10^3 < R_e < 2 \times 10^5$). This flow configuration is considered challenging for the turbulence models, since the boundary layer is laminar and transition to turbulence occurs in the separated shear layers and the wake.

The present investigation aims to access the capabilities of different turbulence modeling techniques for coupled FSI problems. The turbulent test case presented in [6] is simulated employing three different turbulence modeling techniques. The $\zeta - f$ model proposed in [8] is utilized to perform the study in 2-d *Unsteady Reynolds Averaged Navier-Stokes* (URANS) flow simulation. The Smagorinsky model [18] with dynamic procedure suggested by Germano [5] is used to carry out a *Large Eddy Simulation* (LES). A hybrid URANS/LES based on the *Detached Eddy Simulation model* (DDES) [19] with $\zeta - f$ as baseline URANS model, is also tested. The DDES formulation of $\zeta - f$ model has been discussed and verified in [24]. The structural deflections, swiveling frequency and the end mass phase delay from simulations are compared with the experimental data.

2 GOVERNING EQUATIONS

For the fluid subdomain Ω_f, the fluid is assumed to be Newtonian with incompressible fluid motion. The basic conservation equations governing transport of mass and momentum are given as

$$\frac{\partial v_i}{\partial x_i} = 0, \tag{1}$$

$$\rho_f \frac{Dv_i}{Dt} = -\frac{\partial p}{\partial x_i} + \mu_f \frac{\partial^2 v_i}{\partial x_j^2} + \rho_f f_i, \tag{2}$$

where v_i is the velocity vector, p is the static pressure, μ_f is the dynamic fluid viscosity, ρ_f is the fluid density and f_i represent the external force vector.

For the structure subdomain Ω_s, we define a material point X in the reference configuration. The function χ represents the transformation from X to x as

$$x_i = \chi(X_j, t), \tag{3}$$

where X_j are the components of position vector X and x_i represents the components of current spatial position vector x. The displacements are then defined as

$$u_i = x_i - X_i. \tag{4}$$

The basic equation of momentum balance for solid domain Ω_s is written as

$$\rho_s \frac{\partial^2 \chi(X_j, t)}{\partial t^2} = \frac{\partial S_{ji} F_{ij}}{\partial X_j} + \rho_s f_i, \tag{5}$$

where S_{ji} is the second Piola-Kirchhoff stress tensor, ρ_s is the density of solid material and f_s represents the external forces on the solid. $F_{ij} = \partial x_i / \partial X_j$ is the deformation gradient. In the present study, the material is modeled utilizing a simple hyper-elastic material model, the Saint Venant-Kirchhoff law (for details see [16, 23]). For the second Piola-Kirchhoff stress tensor the model states

$$S_{ij} = \lambda_s E_{kk} \delta_{ij} + 2\mu_s E_{ij}, \tag{6}$$

where the Green-Lagrange strain tensor is represented as

$$E_{ij} = \frac{1}{2} \left(F_{ki} f_{kj} - \delta_{ij} \right), \tag{7}$$

with λ_s and μ_s as Lamé constants.

The two subproblems are coupled at the boundary with suitable interface and boundary conditions. The standard boundary conditions apply on the fluid boundaries Γ_f and the structure boundaries Γ_s. The following conditions on velocities and stresses are applied at the fluid-structure interface

$$\left(v_i^f \right)_{\Gamma_f \cap \Gamma_s} = \dot{u}_i^b \quad \text{and} \quad \left(\sigma_{ij}^s \right)_{\Gamma_f \cap \Gamma_s} = \left(\sigma_{ij}^f \right)_{\Gamma_f \cap \Gamma_s}, \tag{8}$$

where $\dot{u}_i^b$ is the velocity of the interface and σ_{ij}^s and σ_{ij}^f represent the Cauchy stress tensor of the solid and the fluid domain, respectively.

3 MODELING APPROACH

This section gives a brief description of turbulence modeling approaches in this study.

3.1 $\zeta - f$ Model

The $\zeta - f$ model proposed in [8] is a linear eddy-viscosity model. The model is capable of predicting the anisotropic behavior of turbulence near walls by evaluating the eddy-viscosity ν_t based on the wall normal velocity scale ratio ζ as $\nu_t = C_\mu \zeta k \tau$, where $\zeta = \overline{v_2'^2}/k$ and k is the kinetic energy of turbulence. The constitutive model equations are given as

$$\frac{Dk}{Dt} = \mathcal{P} - \epsilon + \frac{\partial}{\partial x_i}\left[\left(\nu + \frac{\nu_t}{\sigma_k}\right)\frac{\partial k}{\partial x_i}\right], \tag{9}$$

$$\frac{D\epsilon}{Dt} = \frac{C_{\epsilon 1}\mathcal{P} - C_{\epsilon 2}\epsilon}{\tau} + \frac{\partial}{\partial x_i}\left[\left(\nu + \frac{\nu_t}{\sigma_\epsilon}\right)\frac{\partial \epsilon}{\partial x_i}\right], \tag{10}$$

$$\frac{D\zeta}{Dt} = f - \frac{\zeta}{k}\mathcal{P} + \frac{\partial}{\partial x_i}\left[\left(\nu + \frac{\nu_t}{\sigma_\zeta}\right)\frac{\partial \zeta}{\partial x_i}\right], \tag{11}$$

$$L^2\nabla f - f = \frac{1}{\tau}\left(c_1 + C_2{}'\frac{\mathcal{P}}{\epsilon}\right)\left(\zeta - \frac{2}{3}\right), \tag{12}$$

where ϵ is the dissipation of turbulent kinetic energy, $\mathcal{P}$ is the production of turbulent kinetic energy and f is the elliptic relaxation term that models the pressure-velocity correlations. L and τ are the length and time scales of turbulence, whereas other unknown terms in the given set of equations are model constants. For a detailed model description see [8].

3.2 Dynamic Smagorinsky Model

The LES simulation in this study is performed by applying the Smagorinsky model [18] to estimate the *Sub-Grid Scale* (SGS) turbulent viscosity ν_{SGS} as

$$\nu_{SGS} = C_s\Delta^2|\overline{S}|, \tag{13}$$

where $|\overline{S}| = (2\overline{S_{ij}S_{ij}})^{1/2}$ is the magnitude of strain-rate tensor $\overline{S_{ij}} = \partial\overline{v_i}/\partial x_j + \partial\overline{v_j}/\partial x_i$, C_s is the model constant and $\Delta = (\Delta_1\Delta_2\Delta_3)^{1/3}$ is the filter width, with Δ_i representing filter width in each spatial direction. An overbar on $\overline{S_{ij}}$ represents a filtered quantity.

The model constant $C_s = C_s(x,t)$ is calculated dynamically as proposed by Germano et al. [5]. The resulting equation system to estimate C_s is solved using least squares method as suggested by Lilly [12]. The C_s values are clipped as $C_s(x,t) = \max\{C_s(x,t), 0\}$ to avoid negative values of C_s.

3.3 $\zeta - f$ DDES

The *Detached Eddy Simulation* (DES) concept first proposed by Spalart [20], is to combine URANS and LES to have a model with better prediction of turbulence than a URANS and computationally less expensive than an LES. In the DES approach, the URANS model is modified to achieve a SGS model in regions where grid is fine enough for an LES. The switching between two modes is based on the length scale l_{turb} as

$$l_{turb} = \min(l_{RANS}, C_{DES}\Delta), \tag{14}$$

where $\Delta = \max(\Delta_1, \Delta_2, \Delta_3)$ and C_{DES} is a model constant. l_{turb} is introduced in the URANS model by modifying the dissipation term in the transport equation (9) for the

turbulent kinetic energy as $\epsilon = k^{3/2}/l_{turb}$. l_{turb} either becomes the original URANS length scale ($l_{RANS} < C_{DES}\Delta$) or the SGS length scale ($l_{RANS} > C_{DES}\Delta$).

The Delayed Detached Eddy Simulation (DDES) model was proposed in [19] as an improvement for some deficiencies of the original DES model. The modification and verification of $\zeta - f$ model to perform a DDES are presented in [24]. For DDES, the DES length scale is modified to incorporate a shielding function to preserve the URANS mode in boundary layers, because of the grid clustering near the boundaries $C_{DES}\Delta < l_{RANS}$. A quantity r_d is defined as

$$r_d = \frac{\nu_t + \nu}{\sqrt{v_{i,j}v_{i,j}}\kappa^2 d^2}, \tag{15}$$

where ν is the molecular viscosity, $v_{i,j}$ are the velocity gradients, κ is the Kármán constant and d is the wall distance. The shielding function f_d is defined as a function of r_d as

$$f_d = 1 - \tanh([8r_d]^3). \tag{16}$$

The function f_d is designed to be 0, to prevent activation of LES mode in boundary layer regions. The new length scale for DDES is then defined as

$$l_{DDES} = l_{RANS} - f_d \max(0, d - C_{DES}\Delta\psi), \tag{17}$$

where ψ is the term added to eliminate the influence of low-R_e turbulence models in the SGS mode, which is given as

$$\psi = \sqrt{\left(\frac{C_{\epsilon 1}}{C_{\epsilon 2}C_\mu \zeta}\right)^{3/2}}. \tag{18}$$

4 EXPERIMENTAL SETUP

The structural model for this test case consists of a flexible stainless steel sheet of 0.4 mm thickness, with density $\rho_{flexible\ sheet} = 7855$ kg/m^3 and Young's modulus $E_{flexible\ sheet} = 2\times10^{11}$ N/m^2. The flexible sheet is attached to a revolvable circular cylinder of aluminum. A rectangular stainless steel mass is attached to the other end of the sheet. The physical

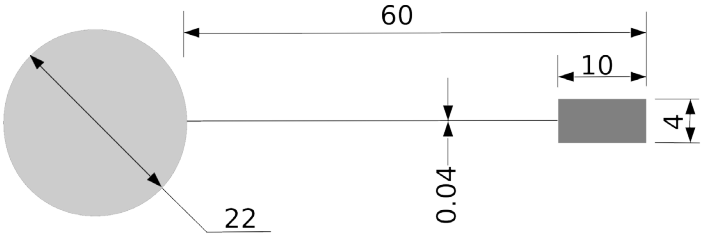

Figure 1: Structural model and dimensions in mm.

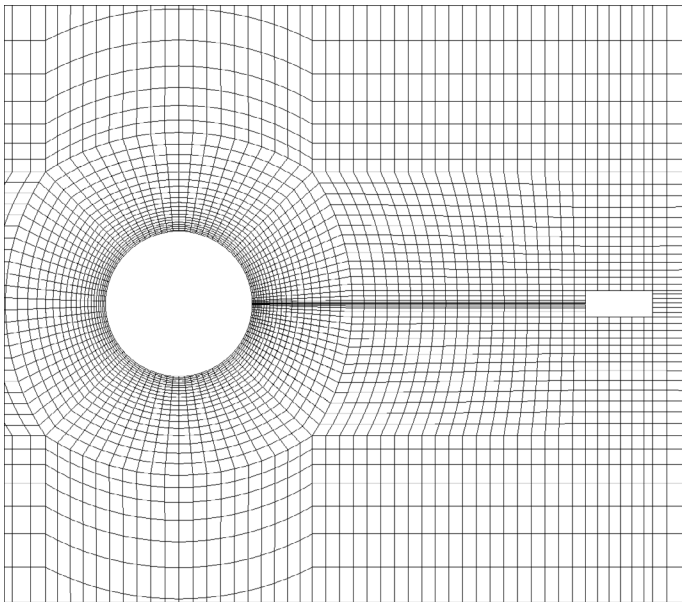

Figure 2: CFD grid around structure.

dimensions and shape of the structure are illustrated in Figure 1. Both, the front cylinder and the rectangular mass, can be considered rigid. The structure is placed inside a vertical tunnel with a test section cross-sectional area of 180 mm $\times$ 240 mm and a length of 338 mm. The fluid is water at 25°C, with kinematic fluid viscosity $\nu_{fluid} = 0.97 \times 10^{-6}$ m^2/s and density $\rho_{fluid} = 998$ kg/m^3. The bulk fluid velocity at the inlet is 0.68 m/s. The structure exposed to the incoming flow velocity oscillates around a mean position, and the flexible sheet deflects in the first mode. The detailed experimental setup, the measurement techniques, and the physical properties of the structure are described in [6].

5 COMPUTATIONAL APPROACH

The structural subproblem is solved employing the finite-element solver FEAP [21]. For the fluid domain, the finite-volume solver FASTEST [13] with block-structured body-fitted grids is used. The parallelization in FASTEST is achieved with domain decomposition and communication via MPI. The data transfer between the two codes and the interpolation on non-matching grid interfaces is performed via the interface coupling code MpCCI [9]. For details concerning the coupling algorithm see [17]. Both, the structural and fluid solver employ fully implicit second-order temporal discretizations. For the spatial discretization, the structural solver involves hexahedra elements with enhanced-strain formulation, whereas the fluid solver utilizes a second-order MUSCL [25] for the 2-d URANS simulation, second-order *Central Differencing Scheme* (CDS) for the LES and a blending between CDS and the GAMMA scheme [10] for the DDES. The blending between two schemes is done via a function introduced in [22], which ensures the calculation of fluxes with the CDS in LES regions and with the GAMMA scheme in RANS regions of

the DDES.

Table 1: Number of CV and time step size

Abbreviation	Turbulence model	No. of CVs	Time step Δt[s]	Averaged no. of periods
Sim-1	$\zeta - f$	0.37×10^6	2.5×10^{-4}	9
Sim-2	$\zeta - f$ DDES	12.0×10^6	1.5×10^{-4}	13
Sim-3	Dyn. Smag.	40.0×10^6	1.5×10^{-4}	7

Table 1 summarize the number of *Control Volumes* (CV), the time step sizes Δt, and the number of motion cycles performed for averaging of the structural deflections. Figure 2 presents a view of the grid used for 2-d URANS (Sim-1), in x-y plane around the structure, where every 4th grid-line is shown. The grids are designed to have $y^+ < 1$, for the first cell adjacent to solid walls. The time step sizes are lower bound by the artificial added mass effect [2]. The convergence of the coupled problem was observed to deteriorate, when reducing the time step size. The CFL number based on the time step sizes varied between 1.4 and 2.0. One reason for large variations in CFL number is the grid movement with structural deflections, where maximum CFL numbers are observed when the structural deflection or the velocity approaches a maximum.

6 RESULTS AND DISCUSSION

The periodic motion of the structure is adequately predicted by the simulations, whereas quantitative comparison among the simulations and the experiment is based on the averaged structural deflections. The averaging is performed in time-phase as suggested in [6], after cycle-to-cycle variations of the end mass displacements reach a minimum. The number of motion periods averaged for each simulation are listed in Table 1.

Figure 3 compares the absolute velocity contours of the experiment and Sim-1 at different phase angles. The arrangement of flow instabilities from the simulation is comparable with the experiment, despite the 2-d approach in Sim-1. Table 2 draws a quantitative comparison for the oscillation frequency of the structure f_{FSI}, the end mass phase delay ϕ_{shift} and y extrema of the end mass normalized by the cylinder diameter. The quantities in Table 2 are time-phase averaged.

The time-phase averaged cylinder rotation angle, and the end mass excursions are plotted in Figure 4a and Figure 4b, respectively. A slight asymmetry in the simulation data can be observed from Table 2 and Figure 4. This asymmetry is more noticeable in Sim-1 and Sim-3, where the motion cycles performed for averaging are less than that of Sim-2. The end mass displacement and the cylinder rotation from Sim-1 are underestimated, with y extrema of the end mass 20% lower than that of experimental values. The overdamping

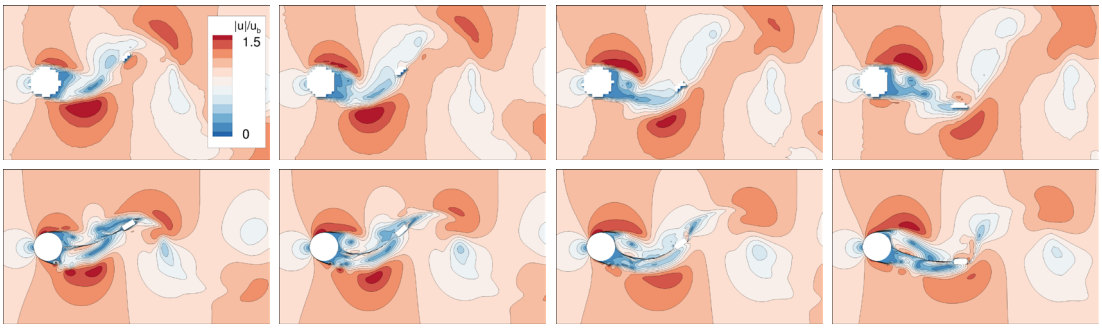

Figure 3: Phase-resolved contours of absolute velocity at different phase angles for Sim-1, comparison of experiment (top) and simulation (bottom).

Table 2: Oscillation frequency, the end mass phase shift and y extrema of the end mass displacement

	f_{FSI}[hz]	ϕ_{shift}[deg]	$(u_y)^*_{max}$	$(u_y)^*_{min}$
GL10 [6]	4.45	95	1.12	-1.11
Sim-1	4.58	109	0.85	-0.90
Sim-2	4.37	84	1.24	-1.25
Sim-3	4.37	83	1.25	-1.26

of the 3-d flow configuration in a 2-d flow simulation can explain the under-prediction of the the structural deflections. A study conducted by Breuer [1] for 2-d simulation of a circular cylinder at $R_e = 3900$, reports the overdamping of turbulent fluid motion.

Sim-2 and Sim-3 exhibit a close agreement in predicted values of the structural deflections. y extrema of the end mass displacement are about 13% higher than the experimental extrema of the end mass. A reason for this pronounced increase in the structural deflections could be the negligence of structural damping. A study of the laminar version of this test case [7] produced good agreement when simulating the *Movement Induced Instability* (MII), whereas large differences are observed for IIE where the structure oscillates in the first mode, as it is the case with this turbulent benchmark test case. The new test cases proposed in [4, 3] (also introduced in Section 1) study the effects of material damping in two different modes of the structural oscillation. The study depicts a higher importance of the material damping in the first mode of the structural oscillation, where the damping model significantly effects the structural deflections in numerical simulation. Nevertheless the material damping for the rubber (used in [4, 3]) would be higher than steel, and the premise that material damping is the cause of the over-prediction in Sim-2 and Sim-3, might not apply. Other possible reason for the differences between simulations

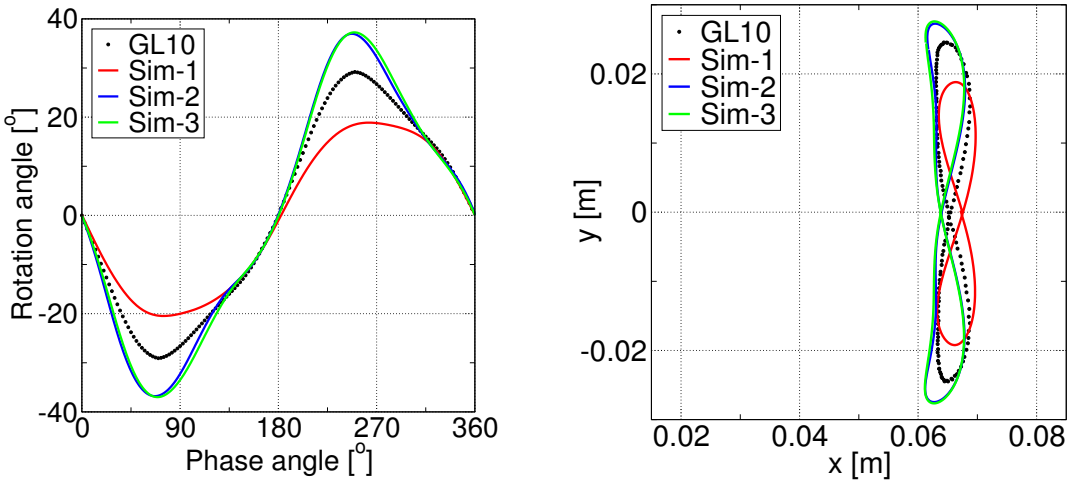

(a) (b)

Figure 4: (a)Cylinder rotation angle plotted against time phase angle. (b)Trailing edge coordinates.

and the experiment could be the ignored side walls, taken as symmetry boundaries in the simulations to reduce the computational cost. The effect of side wall boundary layers are ignored on the assumption that the test section width in experiment is too high (about 8 times the diameter of cylinder) for the side wall boundary layers to have a significant effect.

7 CONCLUSIONS

We have presented the results for a turbulent FSI benchmark test case. Three different turbulence modeling techniques have been studied. The 2-d URANS depicts a reasonable agreement with the experiment, regardless of the 3-d flow configuration. The excessive fluid damping in 2-d URANS is considered to be the cause of underrated structural deflections. The LES and the DDES simulation reproduce a close agreement between each other and an acceptable agreement with the experiment. The probable causes of overestimation of deflection in two simulations are also discussed. Further investigations with a variation of the structural material model are planned, as well as the simulation of the test cases [4, 3] with $\zeta - f$ model.

8 ACKNOWLEDGMENTS

The authors gratefully acknowledge the Research Training Group 1344 of the German Research Foundation for the funding of this project.

REFERENCES

[1] M. Breuer. Large eddy simulation of the subcritical flow past a circular cylinder: numerical and modeling aspects. *International Journal for Numerical Methods in Fluids*, 28(9):1281–1302, 1998.

[2] P. Causin, J.F. Gerbeau, and F. Nobile. Added-mass effect in the design of partitioned algorithms for fluid–structure problems. *Computer methods in applied mechanics and engineering*, 194(42):4506–4527, 2005.

[3] G. De Nayer and M. Breuer. Numerical fsi investigation based on les: Flow past a cylinder with a flexible splitter plate involving large deformations (fsi-pfs-2a). *International Journal of Heat and Fluid Flow*, 50:300–315, 2014.

[4] G. De Nayer, A. Kalmbach, M. Breuer, S. Sicklinger, and R. Wüchner. Flow past a cylinder with a flexible splitter plate: A complementary experimental–numerical investigation and a new fsi test case (fsi-pfs-1a). *Computers & Fluids*, 99:18–43, 2014.

[5] M. Germano, U. Piomelli, P. Moin, and W.H. Cabot. A dynamic subgrid-scale eddy viscosity model. *Physics of Fluids A: Fluid Dynamics (1989-1993)*, 3(7):1760–1765, 1991.

[6] J.P. Gomes and H. Lienhart. Experimental benchmark: Self-excited fluid-structure interaction test cases. In H.J. Bungartz, M. Mehl, and M. Schäfer, editors, *Fluid Structure Interaction II*, volume 73 of *Lecture Notes in Computational Science and Engineering*, pages 383–411. Springer Berlin Heidelberg, 2010.

[7] J.P. Gomes, S. Yigit, H. Lienhart, and M. Schäfer. Experimental and numerical study on a laminar fluid-structure interaction reference test case. *Journal of Fluids and Structures*, 27(1):43 – 61, 2011.

[8] K. Hanjalić, M. Popovac, and M. Hadžiabdić. A robust near-wall elliptic-relaxation eddy-viscosity turbulence model for CFD. *International Journal of Heat and Fluid Flow*, 25(6):1047–1051, 2004.

[9] MpCCI - Mesh-Based Parallel Code Coupling Interface. User guide v3.0. *Fraunhofer, SCAI*, 2004.

[10] H. Jasak, H.G. Weller, and A.D. Gosman. High resolution NVD differencing scheme for arbitrarily unstructured meshes. *International Journal for Numerical Methods in Fluids*, 31(2):431–449, 1999.

[11] A. Kalmbach and M. Breuer. Experimental PIV/V3V measurements of vortex-induced fluid–structure interaction in turbulent flow - A new benchmark FSI-PfS-2a. *Journal of Fluids and Structures*, 42:369–387, 2013.

[12] D.K. Lilly. A proposed modification of the Germano subgrid-scale closure method. *Physics of Fluids A: Fluid Dynamics (1989-1993)*, 4(3):633–635, 1992.

[13] FASTEST - User Manual. Institute of numerical methods in mechanical engineering. *Technische Universität Darmstadt*, 2005.

[14] E. Naudascher and D. Rockwell. *Flow-induced vibrations: An engineering guide*. Courier Dover Publications, 2012.

[15] B.R. Noack. On the flow around a circular cylinder. part ii: turbulent regime. *ZAMM-Journal of Applied Mathematics and Mechanics/Zeitschrift für Angewandte Mathematik und Mechanik*, 79(S1):227–230, 1999.

[16] R.W. Ogden. *Non-linear elastic deformations*. Courier Dover Publications, 1997.

[17] M. Schäfer, D.C. Sternel, G. Becker, and P. Pironkov. Efficient numerical simulation and optimization of fluid-structure interaction. In H.J. Bungartz, M. Mehl, and M. Schäfer, editors, *Fluid Structure Interaction II*, volume 73 of *Lecture Notes in Computational Science and Engineering*, pages 131–158. Springer Berlin Heidelberg, 2010.

[18] J. Smagorinsky. General circulation experiments with the primitive equations: I. The basic experiment. *Monthly weather review*, 91(3):99–164, 1963.

[19] P.R. Spalart, S. Deck, M.L. Shur, K.D. Squires, M.Kh. Strelets, and A. Travin. A new version of detached-eddy simulation, resistant to ambiguous grid densities. *Theoretical and Computational Fluid Dynamics*, 20(3):181–195, 2006.

[20] P.R. Spalart, W.H. Jou, M. Strelets, and S.R. Allmaras. Comments on the feasibility of LES for wings, and on a hybrid RANS/LES approach. In C. Liu and Z. Liu, editors, *Advances in DNS/LES: Proceedings of the First AFOSR International Conference on DNS/LES, Louisiana Tech University, Ruston, Louisiana, USA*. Greyden Press Columbus, OH, August 1997.

[21] R.L. Taylor. Feap - A Finite Element Analysis Program, Version 7.5 User Manual. *University of California at Berkeley, Berkeley, CA*, 2005.

[22] A. Travin, M. Shur, M. Strelets, and P.R. Spalart. Physical and numerical upgrades in the detached-eddy simulation of complex turbulent flows. In R. Friedrich and W. Rodi, editors, *Advances in LES of Complex Flows*, volume 65 of *Fluid Mechanics and its Applications*, pages 239–254. Springer Netherlands, 2002.

[23] C. Truesdell and W. Noll. *The non-linear field theories of mechanics*. Springer, 2004.

[24] S. Türk, T. Reimann, D.C. Sternel, and M. Schäfer. On the performance of detached-eddy simulation in fluid-structure interaction problems. In S. Idelsohn, M. Papadrakakis, and B. Schrefler, editors, *Computational Methods for Coupled Problems in Science and Engineering, COUPLED PROBLEMS 2013*, June 2013.

[25] L. Xue. *Entwicklung eines effizienten parallelen Lösungsalgorithmus zur dreidimensionalen Simulation komplexer turbulenter Strömungen.* PhD thesis, Technische Universität Berlin, 1998.